Enhancing Dexterous Grasping and Manipulation through Linkage-Driven Underactuated Five-Fingered Robotic Hand: A Computational Approach

Deepak R. Biswal [1,*], Pramod K. Parida [2], and Alok R. Biswal [1]

[1] Department of Mechanical Engineering, Dhaneswar Rath Institute of Engineering and Management Studies (DRIEMS) University, Odisha, India

[2] Department of Mechanical Engineering, Odisha University of Technology and Research (Formerly CET), Odisha, India

Email: deepakrbiswal@gmail.com (D.R.B.); pkparida@outr.ac.in (P.K.P.); alokbiswal82@gmail.com (A.R.B.)

*Corresponding author

***Abstract*—This research aims to enhance dexterous grasping and manipulation capabilities through a computational approach involving a novel design of a linkage-driven, underactuated, five-fingered robotic hand. Leveraging underactuated mechanisms, the study addresses the complexity associated with individually actuated joints, offering a streamlined and efficient solution for replicating human-like hand movements. The proposed hand comprises 12 actuators and 21° of freedom, emphasizing the need for enhanced adaptability and reduced complexity in replicating human hand movements. Utilizing SolidWorks for mechanical design, Automated Dynamic Analysis of Mechanical Systems (ADAMS) is employed for dynamic simulations, enabling a comprehensive evaluation of the robotic hand's performance in realistic scenarios. MATLAB is utilized for the required algorithm, and Analysis System (ANSYS) for structural analysis, ensuring the robustness and reliability of the robotic hand under different loading conditions. This approach integrates mechanical engineering principles with advanced simulation tools. The abstract concludes by presenting comprehensive research results, featuring general quantitative data from the entire research process, underscoring the efficacy and applicability of the computational approach in advancing robotic manipulation capabilities.**

***Keywords*—dexterous, five-fingered hand, grasping, linkage-driven, underactuated**

I. Introduction

Underactuated robotic hands represent a pivotal frontier in robotics research, offering a paradigm shift in the pursuit of dexterous and adaptive manipulation. Traditional fully actuated robotic hands face complexity, high energy demands, and limited flexibility when handling various objects. Underactuated hands use fewer actuators than degrees of freedom and rely on passive mechanical structures for varied and energy-efficient movements [1]. This method aligns with human hand biomechanics and offers a promising way to enhance robotic interaction with the real world.

By building and evaluating a linkage-driven underactuated five-fingered robotic hand, this study aims to advance the field of robotic manipulation. The primary goal is to improve the dexterous gripping and manipulation skills of the hand using a computational approach. It is intended to optimize the mechanical design for adaptability, simulate the dynamic scenarios in order to test the performance, and to undertake the structural analysis to assure the robustness by integrating SolidWorks, Automated Dynamic Analysis of Mechanical Systems (ADAMS), and Analysis System (ANSYS) software. This study aims to provide significant insights into the design ideas and computational tools required for achieving exceptional dexterity in underactuated robotic hands while addressing real world issues. The purpose of this research is to enhance dexterous grasping and manipulation using a linkage-driven underactuated five-fingered robotic hand through a computational approach. The benefit of this research lies in advancing the capabilities of robotic manipulation, potentially leading to more versatile and efficient robotic systems capable of handling a wide range of objects in various environments.

Some of the important research in this regard are highlighted. A linkage driven three fingered underactuated robotic hand designed to mimic the flexion and extension, abduction and adduction movement of a human hand was proposed by Li *et al.* [2]. In their work, the authors described the robotic hand's components, such as the underactuated fingers, underactuated planar linkage, spherical four bar mechanism, and bevel-gears. A review on the multi-fingered robotic gripper is presented by

Manuscript received January 23, 2024; revised April 7, 2024; accepted April 30, 2024; published October 25, 2024.

Parveen *et al.* [3]. In this paper, author comprehensively review various robotic multi-finger grippers, examining their geometrical information, degrees of freedom, grasping systems, and usability for understanding anthropomorphic hand. Additionally, they delve into the latest technological developments and experiments within the field of robotic grippers in real-world applications. On adaptive grasp with underactuated anthropomorphic hands was proposed by Chen *et al.* [4]. The objective of this paper was to formulate a design methodology for underactuated anthropomorphic hands, ensuring their dependable adaptation to various grasped objects. Concurrently, authors aim to devise an analytical approach to examine the progression of motion and force throughout the entirety of the underactuated grasping process.

The design of several elastic actuators and an enhanced controller for such actuators were discussed by Chauhan *et al.* [5] to regulate the motion of a user's hand in a linkage based hand exoskeleton. The article lacks a comparison between the proposed series elastic actuator and other types of actuators commonly used. Design and improvement of a linkage as well as tendon operated human like five fingered robot hand is proposed by Yang *et al.* [6]. This paper outlines the design of the proposed robotic hand and establishes the kinematics of its linkage and tendon-driven fingers, subsequently characterizing the hand's workspace and investigating thumb opposability. To improve the design characteristics of the robot finger, the researchers used dynamic simulation models and response surface methods [7, 8]. A Three-Finger Robot Hand with Human-Like Flexion, which is underactuated was proposed by Kwon *et al.* [9]. They used ADAMS software to create a dynamic simulation model of a robot finger, refining critical design elements like spring coefficients for human-like movements. Experimental validation of optimization results suggests the potential for prosthetic fingers mimicking human hand movements. A mathematical study of contact-forces for the under-actuated finger in an underactuated robotic-hand at grasping is presented by Ha *et al.* [10].

A study on investigating the force distribution involved in the thumb-index finger power-grasp while holding fruit is presented in [11]. Though the work mentions significant differences in force distribution, it presents an opportunity to enhance clarity by including specific numerical data and effect sizes. Improvement and enactment of a five-fingered human like underactuated prosthesis with adaptive grasp was presented by Estay *et al.* [12]. While the prosthetic hand demonstrates impressive capabilities, its potential limitation lies in the precision of finger control, particularly noticeable during tasks such as holding a needle, which require a higher level of accuracy beyond the prosthesis's current capabilities. An underactuated robotic-hand with a thumb and two fingers for grasping is presented by Li *et al.* [13]. The thumb consists of two joints with two degrees of flexibility that are controlled by a single motor. This study demonstrates that an underactuated hand can replicate most of the human hand's gripping behaviors. A review on linkage-driven finger mechanisms for prosthetic use was designed and proposed by Kashef *et al.* [14]. The paper outlines existing literature and reviews linkage-driven fingers but unable to propose novel approaches or advancements in artificial finger design beyond those already discussed. In 2022, Bao and Takakai [15] proposed a lightweight, high-output manipulator comprising a robot hand and wrist. Their innovative design utilizes a differential mechanism to combine actuator output forces, doubling force output while maintaining low power consumption. Integration of a driving force amplification device in the wrist enhances finger gripping force. This research yields a manipulator facilitating rapid and secure object grasping. A soft robotic gripper powered by flexible shafts is presented for combined grabbing and in-hand manipulation [16]. The study highlights the challenge of uncertain object manipulation in unstructured environments however it doesn't specify the exact nature of these challenges and doesn't provide a detailed comparison between rigid and soft grippers. To assess the usual standards for grip power and finger forces in order to assist clinical practice in terms of assessing hand strength in patients who sustained hand fractures was analysed by Keller *et al.* [17]. The study does not address dynamic aspects of hand function, such as variability in force exertion, speed of movement.

An underactuated gripper with passive compliance and grasping force sensing capabilites is introduced by Ruiz *et al.* [18]. Their design features elastic connections replacing rigid ones for compliant gripping. Joint torques and grabbing forces are estimated based on the compression of these elastic connections, combined with the gripper's model and joint angle sizes. Carabelo *et al.* [19] investigated a test setup and procedure to validate the maximum finger contraction force based on finger position in flexion and active fingers. The study concludes that the configuration should be portable and flexible for everyday use. Kim *et al.* [20] developed an Integrated Linkage Driven Dexterous Anthropomorphic (ILDA) hand that can perform dexterous tasks similar to human hands. The ILDA hand, developed using a linkage-driven mechanism, incorporates all necessary components for actuation and sensing. It achieves 3 degrees of freedom in finger movements through a combination of parallel and series mechanisms. Design and analysis of multi-finger robotic hand is presented by Flaieh *et al.* [21]. The objective of this research was to enhance the grasping and manipulation capabilities of robotic hands, particularly focusing on underactuation for automatic adaptation to object shapes.

Gifu-Hand II, an anthropomorphic robotic hand with a thumb and four fingers was introduced .The thumb has four degrees of freedom , the other fingers have four degrees of freedom and two axes of the joints near the palm orthogonally cross at one point, like in the human hand [22]. He *et al.* [23] proposed a review of underactuated robotics, examining the present state of the art. The study identifies and summarizes underactuated robots and their common mechanisms, using the non-holonomic constraint equation as a starting point. Additionally, the controllability of underactuated robots

was further investigated. KULEX-hand an underactuated exoskeleton was suggested by Hong *et al.* [24] to assist individuals with partially paralyzed or weak hands in improving grasping abilities. The exoskeleton utilizes underactuated fingers, power transmission devices, and a passive thumb link to mimic natural hand motion. The researchers also conducted efficiency studies on the prototype. Progress of a three fingered multifaceted skilful robot hand with combined sensors was proposed by Chen *et al.* [25]. While precision experiments are conducted on force/torque sensors and joint movements, there's no mention of real-world application tests. The performance analysis of an adaptive thumb mechanism, which has three degrees of freedom, was presented by Li *et al.* [26]. The text could enhance its contribution by including a comparative analysis between the performance of the developed dexterous hand and existing similar systems.

A comparison of an actuation and under-actuation of Robotic Hands was proposed by DuFrene [27]. This research aims to compare puppetted and teleoperation control of robotic hands using the Asterisk test. Modified versions of Model Q and Model W were tested, revealing differences in accuracy and completion smoothness, particularly noticeable in the underactuated Model Q during teleoperation. Stability analysis and optimal enveloping grasp planning were proposed by Li *et al.* [28]. Grip stability was discussed in this study. The design and analysis of an ideal encircling grasp for a Deployable Robotic Hand (DRH) were examined. A method for determining the encircling grasp stability evaluation index was constructed. Additionally, an optimal all-encompassing grasp planning approach was proposed to achieve the desired DRH deployment length and ensure a solid grip.

Despite considerable advancements, there remain inherent challenges associated with the design, control, and functionality of underactuated robotic hands. This research aims to address these challenges by proposing linkage driven design to enhance the performance and dexterity of such systems. In this proposed work a five-fingered robot hand is designed. The hand consists of five fingers, similar to a human hand. The thumb is present opposite to the remaining four fingers. The movement of all the fingers are governed by a linkage-driven underactuation concept. All the fingers of the hand comprises of 21° freedom with 12° of actuation. The proposed robotic hand is modelled on a solid work platform, taking the dimensions with reference to the human hand. Contact force equations are being established. The hand is grasping an object with all its distal phalynx in contact. A Matrix Laboratory (MATLAB) code is established, and the contact force of the distal phalynx with the object is validated with the existing work. Simulation of the hand is carried out on the ADAMS platform while grasping the object. Further analysis is carried out on the ANSYS platform to study the structural analysis.

II. Material and Method

The five-fingered robotic hand is modelled on a solid work platform in light of the dimensions of a human hand. All four fingers and the thumb are considered as individual manipulators. The materials used for the hand model are stainless steel and aluminum alloy. The development process of the five-fingered robotic hand involves meticulous attention to detail, starting with its design on a SolidWorks platform. This design phase precisely takes into account the dimensions and proportions of the human hand, ensuring that the robotic hand closely resembles its natural counterpart. Notably, each of the five fingers, including the thumb, is precisely modeled as individual manipulators, allowing for intricate and precise movements akin to human hand dexterity.

Stainless steel and aluminum alloy were chosen for the robotic hand based on their specific properties aligning with the application's requirements. Stainless steel offers high strength and corrosion resistance, ensuring durability under mechanical stress and diverse environmental conditions. This makes it well-suited for critical load-bearing components of the hand. Meanwhile, aluminum alloy's lightweight nature enhances maneuverability without compromising structural integrity. Their combined use optimizes weight distribution and rigidity, critical for precise movements and long-term reliability. This selection balances strength, durability, and weight, essential for the hand's structural performance. The implications of these material choices extend to the hand's ability to maintain structural integrity under varying stress levels, ensuring consistent functionality and resilience throughout its operational lifespan. By combining advanced engineering principles with a keen understanding of human anatomy, the resulting robotic hand achieves a remarkable level of functionality and versatility, making it suitable for a wide range of applications in robotics and automation. A solid work platform is used to model the hand, and simulation is carried out on the ADAMS platform. The algorithm is established in MATLAB environment, and the structural analysis is performed in ANSYS.

III. Design Methodology

The design methodology includes the design of a single finger and finally the hand. The single finger comprises the linkage-driven underactuation mechanism for its operation. The hand comprises five fingers, which includes four fingers and a thumb as in a human hand.

A. Design of the Finger

A single finger of the robot hand that is driven by a linkage mechanism is presented in Fig. 1. The three phalanges of an individual finger are operated by two actuators. Both actuators are present at the Metacarpophalangeal (MCP) joint. One actuator is used for the flexion and extension of the three digits of the finger, and other actuator is used for the abduction and adduction motion of the finger. The four-bar linkage mechanism is used for the flexion and extension of the finger.

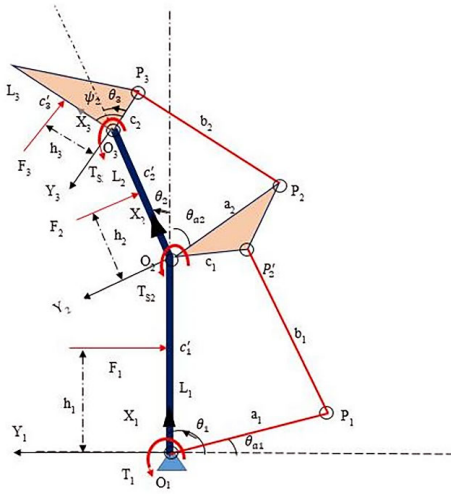

Fig. 1. Layout of the finger.

In Fig. 1, L_1, L_2, and L_3, represents the lengths of the proximal, middle and distal link. a_1, b_1 and c_1 stands for first driving bar, first underactuated bar and second driving bars of the four bar linkage $O_1O_2P'_2P_1$ respectively. The link a_2, b_2, and c_2 stands for second driving bar, second underactuated bar and second driving bars of the four bar linkage $O_2O_3P_3P_2$.The motion begins with the rotation of the input link, also known as the driving bar a_1 which is typically actuated by a motor or another driving force. This rotational motion of the input link is controlled and regulated based on the desired movement of the robot hand, such as grasping an object or adjusting finger position. As the driving bar rotates, it transmits motion to the first underactuated bar b_1 through interconnected joints. The motion is then transmitted to the second driving bar c_1 of the fourbar linkage $O_1O_2P'_2P_1$, causing the middle link L_2 to bend. Subsequently, the motion is transferred to the second driving bar c_2 of the fourbar linkage $O_2O_3P_3P_2$ and then to the second underactuated bar a_2 and finally to the second driving bar c_2 through the second underactuated bar b_2. As a result, the distal link L_3 rotates toward the object for grasping. The motion of the input link, and consequently, the entire mechanism, is controlled and regulated based on the robot's programming and sensor feedback.

The Computer-Aided Design (CAD) model of the finger model is presented in Fig. 2. The flexion/extension of a single finger is illustrated from the starting position to ending position.

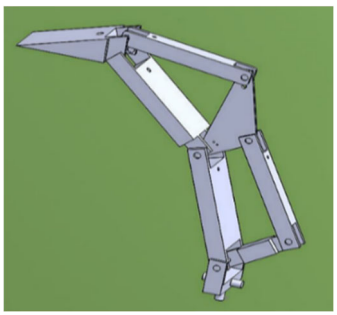

(a)

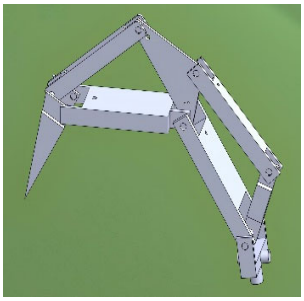

(b)

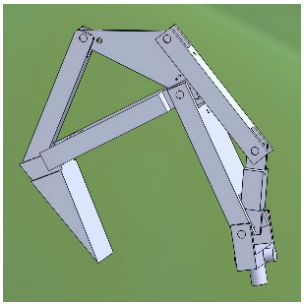

(c)

Fig. 2. Model of a single finger movement at (a) beginning of grasping, (b) middle of grasping, (c) end of grasping.

At the MCP joint two motors are present. One motor can control flexion/extension, while the other controls abduction/adduction. Control algorithms are developed to coordinate the motion of both motors simultaneously, ensuring smooth and synchronized movement. The control system receives input signals or commands specifying the desired motion for both flexion/extension and abduction/adduction. The control algorithm then calculates the appropriate control signals for each motor to achieve the desired motion while ensuring coordination between the two motions. Synchronization between the two motors is crucial to ensure that flexion/extension and abduction/adduction motions occur simultaneously and smoothly. The control algorithm may incorporate synchronization mechanisms that adjust the speed and timing of each motor's motion to maintain coordination.

B. Design of the Hand

The proposed hand design consists of a total of five digits, comprising four standard fingers and a distinct thumb. The total hand comprises 21° of freedom and 12 actuators for efficient operation. Each individual finger possesses 4° of freedom, and requires two actuators for control. Collectively, the four fingers boast eight actuation degrees, allowing for versatile movement, while offering a combined total of 16° of freedom. In contrast, the thumb exhibits 4° of actuation and 5° of freedom, granting it a unique range of motion.

For further insight into the intricate mechanics of the hand's components, a detailed Computer-Aided Design (CAD) model of one of the hand is provided in Fig. 3, facilitating a visual representation for analysis and comprehension. The five-fingered hand holding a truncated shaped object is presented in Fig. 4.

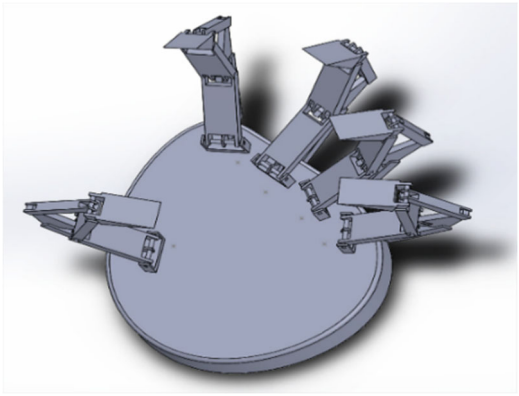

Fig. 3. Model of the hand.

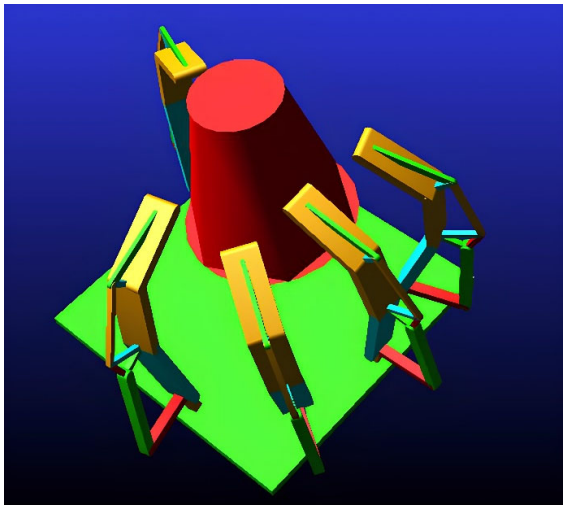

Fig. 4. Hand grasping an object.

C. General Contact Force Analysis of Underactuated Finger

The general equations of motions of virtual input and output power is presented in Eq. (1) as follows.

$$T^T \omega_a = F^T v \tag{1}$$

where T^T is the torque, ω_a is the angular velocity, F^T is the contact force and v is the projected velocity.

In Eq. (1), $v = J_T \dot{\theta}$ and $\dot{\theta} = J_A \omega_a$, where J_T is the Jacobian matrix that relates joint velocities to end-effector velocities, and J_A is the actuation Jacobian matrix incorporates mechanical design and actuation mechanisms, providing a more refined representation for control algorithms and $\dot{\theta} = d\theta/dt$.

Putting the values of v and $\dot{\theta}$ in the Eq. (1) and simplifying, the Eqs. (2)–(4) will be obtained which are as follows.

$$T^T \omega_a = F^T v = F^T J_T \dot{\theta} = F^T J_T J_A \omega_a \tag{2}$$

$$T^T = F^T J_T J_A \tag{3}$$

$$T^T J_A^{-T} = J_T F^T \tag{4}$$

The value of $T^T J_A^{-T}$ and $J_T F^T$ are presented in Eqs. (5) and (6).

$$\begin{bmatrix} \tau_1 \\ \tau_2 \\ \tau_3 \\ \dots \\ \tau_n \end{bmatrix} = T^T J_A^{-T} = \begin{bmatrix} T_1 \\ T_{S2} - X_1 T_1 \\ T_{S3} - X_2 T_{S2} + X_1 X_2 T_1 \\ \dots \\ T_{Sn} + \sum_{j=1}^{n-1} [(-1)^{n-j} \coprod_{i=j}^{n-1} X_i T_{Si}] \end{bmatrix} \tag{5}$$

$$J_T F^T = \begin{bmatrix} h_1 & 0 & 0 & \dots & 0 \\ \alpha_{12} & h_2 & 0 & \dots & 0 \\ \alpha_{13} & \alpha_{23} & h_3 & \dots & 0 \\ \dots & \dots & \dots & \dots & \dots \\ \alpha_{1n} & \alpha_{2n} & \alpha_{3n} & \dots & h_n \end{bmatrix} \begin{bmatrix} F_1 \\ F_2 \\ F_3 \\ \dots \\ F_n \end{bmatrix} \tag{6}$$

Now the equations of motion can be presented in Eq. (7).

$$\begin{bmatrix} h_1 & 0 & 0 & \dots & 0 \\ \alpha_{12} & h_2 & 0 & \dots & 0 \\ \alpha_{13} & \alpha_{23} & h_3 & \dots & 0 \\ \dots & \dots & \dots & \dots & \dots \\ \alpha_{1n} & \alpha_{2n} & \alpha_{3n} & \dots & h_n \end{bmatrix} \begin{bmatrix} F_1 \\ F_2 \\ F_3 \\ \dots \\ F_n \end{bmatrix} = \begin{bmatrix} \tau_1 \\ \tau_2 \\ \tau_3 \\ \dots \\ \tau_n \end{bmatrix} \tag{7}$$

The Eq. (7) can be presented in Eq. (8) as below.

$$\sum_{j=i}^{j=n} \alpha_{ij} F_j = \tau_i, \; \alpha_{ii} = k_i \tag{8}$$

In 1st case when all the three phalanges are in touch with the object and the contact force can be represented as Eq. (9).

$$\begin{bmatrix} h_1 & h_2 + L_1 C_2 & h_3 + L_1 C_{23} + L_2 C_3 \\ 0 & h_2 & h_3 + L_2 C_3 \\ 0 & 0 & h_3 \end{bmatrix} \begin{bmatrix} F_1 \\ F_2 \\ F_3 \end{bmatrix} = \begin{bmatrix} T_1 \\ T_{S2} - X_1 T_1 \\ T_{S3} - X_2 T_{S2} + X_1 X_2 T_1 \end{bmatrix} \tag{9}$$

In 2nd case, when the object is in contact with the proximal and distal phalanges only the contact force can be evaluated as Eq. (10).

$$\begin{bmatrix} h_1 & h_3 + L_1 C_{23} + L_2 C_3 \\ 0 & h_3 \end{bmatrix} \begin{bmatrix} F_1 \\ F_3 \end{bmatrix} = \begin{bmatrix} T_1 \\ T_{S3} - X_2 T_{S2} + X_1 X_2 T_1 \end{bmatrix} \tag{10}$$

In the 3rd case, when the distal and the middle phalanges are in contact with the object the contact force with the object will be presented as Eq. (11).

$$\begin{bmatrix} h_2 & h_3 + L_2 C_3 \\ 0 & h_3 \end{bmatrix} \rightleftarrows \begin{bmatrix} F_2 \\ F_3 \end{bmatrix} = \begin{bmatrix} T_{S2} - X_1 T_1 \\ T_{S3} - X_2 T_{S2} + X_1 X_2 T_1 \end{bmatrix} \tag{11}$$

In 4th case, finally the distal phalynx only contacts the object, and the force of contact will be presented as Eq. (12).

$$[h_3][F_3] = [T_{S3} - X_2 T_{S2} + X_1 X_2 T_1] \tag{12}$$

D. Validation of the Present Formulation

The chapter initially presents the validation of the developed computer code, which is capable of analysing the force of contact in a single underactuated robotic finger with consideration of four cases. Validation for contact force in an underactuated single-finger linkage-driven hand is carried out when only the distal phalange is in contact with the object. The material used for the hand and

the cylinder is aluminium. The torque applied at the 1st driving bar of the 1st four-bar linkage is 1.0 N·m, 1.5 N·m, and 2.0 N·m. Respectively. The contact force obtained at the proximal, middle, and distal phalanges are F_1, F_2, and F_3. The result is validated using a MATLAB code. The value of the contact force obtained considering all four cases by applying the above values of torque is presented in the table below. The comparative result indicates that the contact forces are nearly equal. The contact force of the proposed hand model is validated with the existing work, and the comparison plot is presented in the Fig. 5. It is observed from the plot that the contact-force of the distal phalynx of the finger with the object is approximately close to the existing plot.

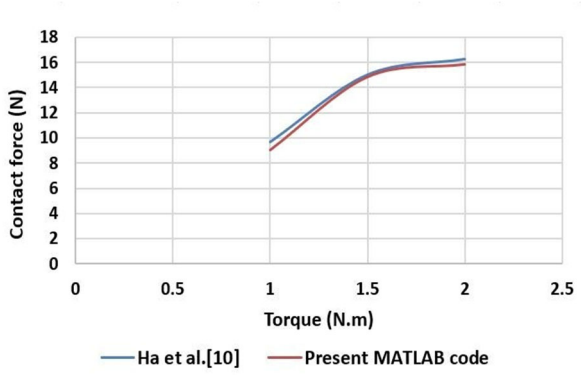

Fig. 5. Validation of the contact force analysis.

The observed contact forces offer insights into the distribution of load among the fingers during grasping. Additionally, analysing the torques exerted on each finger joint provides valuable information about the mechanical demands and stress distribution within the robotic hand.

IV. Result and Discussion

The proposed hand is modelled on a solid work platform, and the mechanism of operation is simulated in various software programs. When the hand touches the object, contact is established with the phalanges of the fingers. Each individual finger consists of kinematic links, or phalynx. The contact force analysis of a single finger is carried out. A single finger comprises three phalanges, i.e., the distal, middle and proximal. The object is in contact with the distal phalynx of the finger in the present analysis.

A. Analysis for the Contact Forces

The contact force analysis of a linkage-driven, underactuated robotic hand is elaborated. The plot is drawn between the contact forces, the angle between the proximal and middle phalynx (θ_2), and the angle between the middle and distal phalynx (θ_3) of a single underactuated finger. By writing MATLAB code for the equations as mentioned, the surface plots are obtained. The angles θ_2 and θ_3 have varied from −100° to 100 °. The plotted graph is presented in Fig. 6.

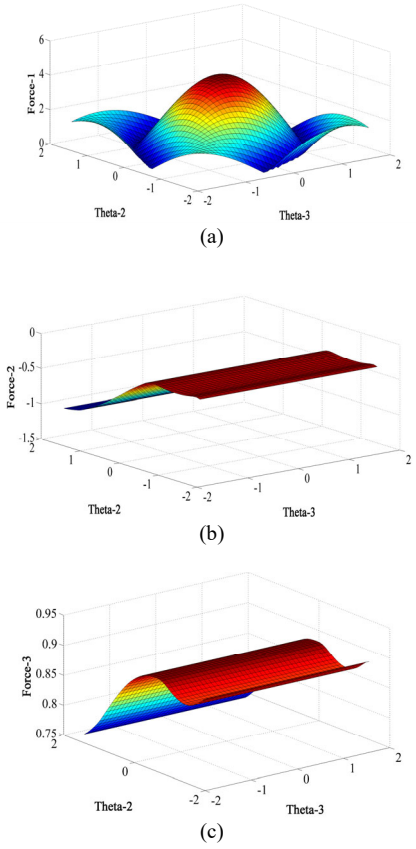

Fig. 6. Contact force plot. (a) Proximal-phalynx; (b) middle-phalynx; (c) distal-phalynx.

The angles θ_2 and θ_3 represents the joint angles of the robotic finger at PIP and DIP joint. These angles play a crucial role in determining the orientation and posture of the finger during grasping and manipulation tasks. As these angles vary, they induce changes in the mechanical configuration of the finger, thus impacting the distribution of contact forces along its surface. An increase in θ_2 may result in a greater bending of the finger, thereby altering the distribution of forces exerted at different contact points. Similarly, changes in θ_3 could affect the curvature of the finger, influencing how contact forces are distributed along its length. A more uniform distribution of contact forces along the finger may enhance stability during grasping, ensuring a secure hold on objects of various shapes and sizes. Conversely, uneven distribution of forces might lead to instability or inefficient manipulation, affecting the dexterity and performance of the robotic hand. Referring to Fig. 6(a), it has been observed that as the values of θ_2 and θ_3 change from −100° to 100°, the force of contact F_1 will change from −1.2 N to −0.2 N accordingly. Similarly, the contact force between the body and the middle phalynx F_2 has been presented in Fig. 6(b) with variations of θ_2 and θ_3 from −100° to 100°. From the figure, it is found that the contact force F_2 changes its value from 0.75 N to 0.95 N as the angles θ_2 and θ_3 vary from −100° to 100°. The contact force between the body and the distal phalynx, i.e., F_3, is presented in Fig. 6(c).

B. Dynamic Simulation

A five-finger, underactuated robotic hand is intended for grabbing various types of objects. The hand is built with the measurements of a human hand in mind. The hand in the illustration is holding a truncated-shaped object. The investigation of various mechanical factors is illustrated. The underactuated robotic hand is one that is driven by a linkage-driven mechanism. The truncated-shaped object is in fingertip contact with all five fingers of an underactuated robotic hand. The tip of the distal phalynx of all five fingers is in contact with the object only.

The size of the truncated object is: the base circle diameter is 40 mm, the top circle diameter is 20 mm, and the length of the axis is 60 mm. The truncated object is in contact with all the fingertips, considering the coulombs friction. The duration of the simulation is 0.3 s, with a step size of 0.001. The contact forces and torques are analysed and presented in the table. It is observed that the forces obtained from the simulation. The force and torque at first increase and remain constant for the duration of the simulation. The result of the dynamic simulation is presented in Fig. 7. The contact forces of the fingers with the truncated-shaped object for all the fingers are plotted. During the contact of the distal phalanges of all five fingers with the object, contact forces will be established. For the equilibrium of the object, it is necessary to apply forces in all directions. Variations in forces occur during the contact of the phalanges to maintain the body in equilibrium. Fig. 7(a) represents the variation of the contact force of an individual finger. From the plot, it is observed that the magnitude of the contact force initially increases to 13 N, then decreases to nearly 5 N, remains constant for some time, and gradually decreases thereafter. Similarly, the contact force for all fingers is presented in Fig. 7(b–e). The torque for contact-1 is illustrated in Fig. 7(f). The plot demonstrates that the torque value increases to 0.55 N·m and then decreases to 0.2 N·m, and then remain constant for some period before further gradual decrease.

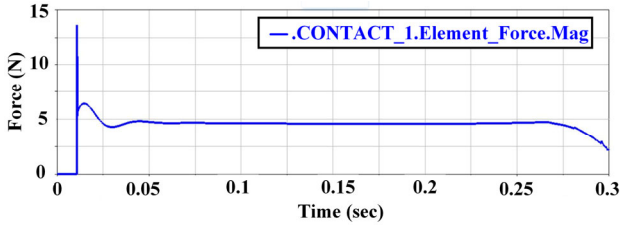

(a)

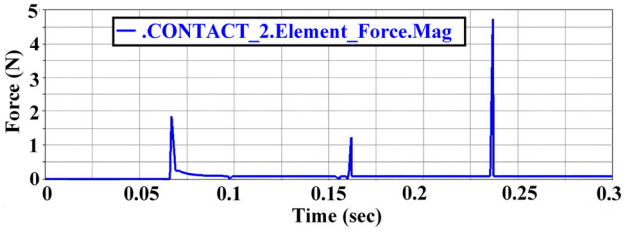

(b)

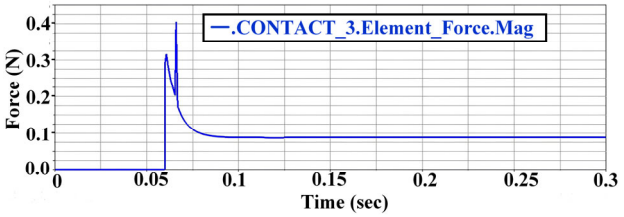

(c)

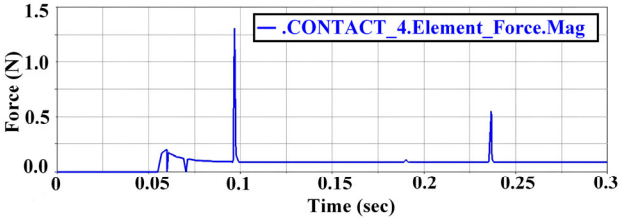

(d)

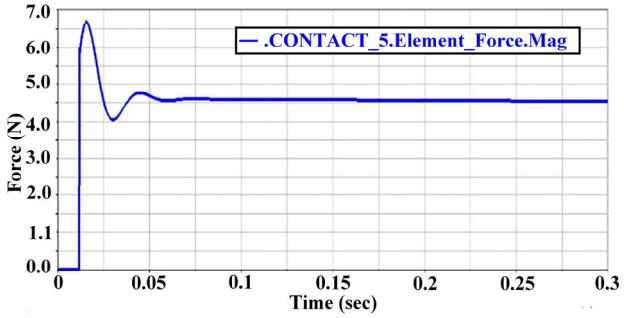

(e)

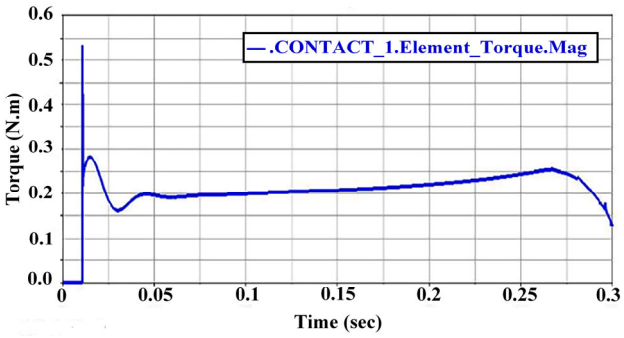

(f)

Fig. 7. Simulation plot in ADAMS for (a) contact force1;(b) contact force2; (c) contact force3; (d) contact force4;(e) contact force5;(f) contact torque1.

A. Structural Analysis

The structural analysis was conducted using the ANSYS environment, a sophisticated software platform renowned for its robust capabilities in engineering simulations. Within this analysis, a force of 200 N was specifically applied at the distal face of the structure under scrutiny. Both stainless steel and aluminium alloy were chosen as materials for the analysis, indicating a comprehensive examination of materials with differing properties. To accurately represent the intricate geometry of the structure, triangular meshing was employed, a method known for its mesh quality, flexibility, adaptability, effectiveness in capturing complex shapes and ensuring precise computational results. The model

encompassed a total of 41 active bodies, reflecting the complexity and diversity of components within the system. The meshing process comprises of 40,930 nodes and 18,469 elements meticulously representing the structure's geometry and enabling thorough analysis of stress and strain distributions throughout the system. The analysis included a deformation analysis segment focused on both stainless steel and aluminium alloy materials, presenting a comparative evaluation of their respective responses to applied loads and resulting deformations. This aspect underscores the importance of understanding material behaviour under various conditions for informed decision-making in engineering design and optimization.

Finally, the outcomes of the structural analysis conducted within the ANSYS environment were visually depicted in Figs. 8–10, offering a concise representation of critical findings such as stress concentrations, deformation patterns, and structural integrity assessments. These results serve as valuable insights for further design refinements, performance enhancements, and validation efforts.

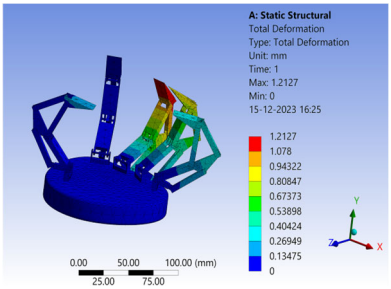

(a)

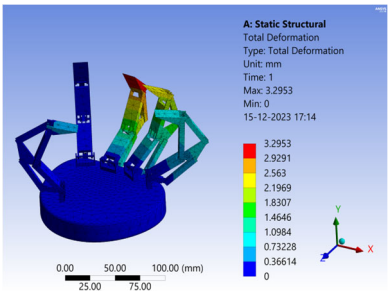

(b)

Fig. 8. Analysis of total deformation for (a) stainless steel and (b) Al-Alloy.

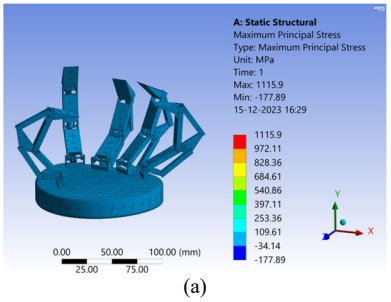

(a)

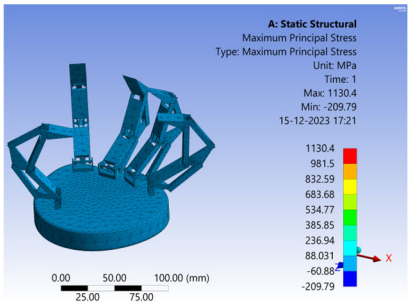

(b)

Fig. 9. Analysis of maximum principal stress for (a) stainless steel and (b) Al-Alloy.

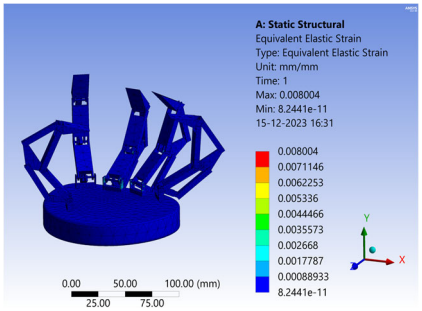

(a)

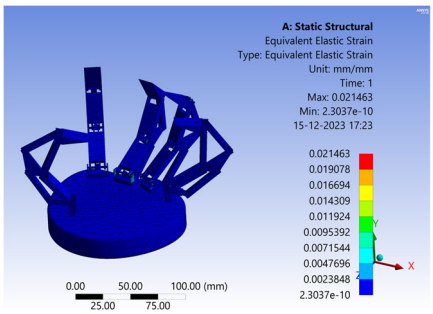

(b)

Fig. 10. Analysis of equivalent elastic strain for (a) stainless steel and (b) Al-Alloy.

The comparison of the mechanical parameters is presented in Fig. 11. The mechanical parameters analyzed are total deformation, principal stress, and elastic strain. The comparison of these mechanical parameters offers a comprehensive overview of how the structure responds to various loading scenarios and material properties. By examining trends and disparities in total deformation, principal stress distribution, and elastic strain across different sections or materials within the structure, informed decision can be made regarding design modifications, material selection, and structural optimization to enhance performance, durability, and safety.

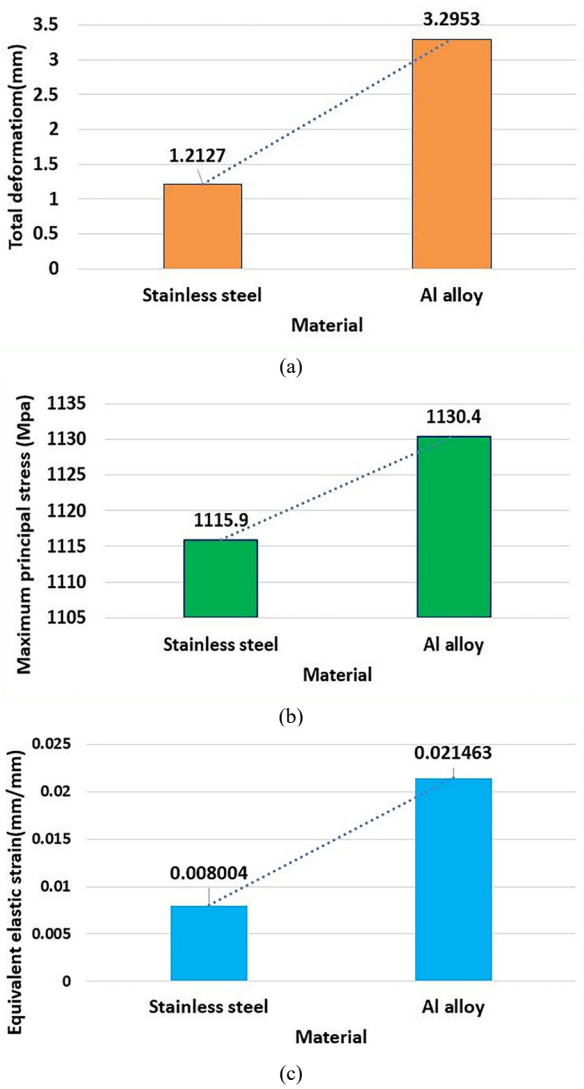

Fig. 11. Comparisons of the mechanical properties (a) total deformation, (b) maximum principal stress (c) equivalent elastic strain.

The analysis reveals notable differences in the response of the robotic hand's distal phalanx when subjected to the same applied load, depending on whether it is constructed from stainless steel or aluminium alloy. Specifically, when the load is applied to the distal phalanx, the observed deformation differs significantly between the two materials. For stainless steel, the deformation measures 1.2127 mm, while for aluminium alloy, it measures 3.2953 mm. These findings, illustrated in Fig. 11(a), highlight the varying levels of flexibility and stiffness exhibited by the two materials under the imposed load. Furthermore, the maximum principal stress values experienced by each material provide crucial insights into their structural integrity and susceptibility to mechanical failure. In Fig. 11(b), it is depicted that the maximum principal stress value for stainless steel reaches 1115.9 MPa, while for aluminium alloy, it is slightly higher at 1130.4 MPa. This suggests that, despite the differences in deformation, both materials endure substantial stress concentrations, with aluminium alloy experiencing slightly higher stress levels compared to stainless steel. Additionally, the equivalent elastic strain values offer further understanding of the materials' ability to undergo reversible deformation within their elastic limits. As shown in Fig. 11(c), stainless steel exhibits an equivalent elastic strain of 0.008004 mm, while aluminium alloy demonstrates a higher value of 0.021463 mm. This indicates that aluminium alloy undergoes more significant elastic deformation compared to stainless steel under the applied load, potentially due to its lower modulus of elasticity. Overall, these findings underscore the importance of material selection in ensuring the desired mechanical performance and structural integrity of the robotic hand's components. Factors such as deformation, stress distribution, and elastic behaviour must be carefully considered when designing and optimizing robotic systems to meet functional requirements and performance objectives.

V. Conclusion

The development of a five-fingered linkage-driven underactuated robotic hand represents a significant leap forward in robotic engineering. The proposed linkage-driven underactuated robotic hand is capable of handling various types of objects in daily life. With 12 actuators and 21° of freedom, it skilfully grasps objects. This mechanism is favourable due to its simplicity in control, providing a firm grasp compared to alternative methods like tendon-pulley and gear driven attachments. Through the integration of SolidWorks and ADAMS, meticulous design, simulation, and analysis have resulted in a hand boasting enhanced performance and versatility. The underactuated nature allows for efficient adaptation to diverse grasping scenarios, closely resembling human dexterity and setting it apart from traditional designs. This uniqueness broadens its potential applications across various industries. The seamless transition from virtual design to dynamic simulations facilitated by SolidWorks and ADAMS offers invaluable insights into the hand's behaviour, ensuring optimal functionality. Additionally, structural analysis conducted via the ANSYS platform further validates its robustness and reliability. By emphasizing its distinctive features and discussing potential applications, this research underscores the hand's significance in advancing robotics for precise manipulation tasks. The success value of our research towards the expected objectives, would be approximately 80%. It not only demonstrates real-world potential but also showcases the ongoing evolution of robotic technology towards more efficient solutions.

Conflict of Interest

The authors declare no conflict of interest.

Author Contributions

DRB conducted conceptualization, designed methodology, developed the core computational models, conducted formal analysis, conducted validation, analysed simulation and conducted writing - original draft; PKP conducted supervision, conducted data curation, designed methodology, conducted conceptualization, conducted

writing - review & editing, revised the manuscript ; ARB managed software, checked visualization, designed methodology conducted conceptualization, conducted computational simulation, and conducted writing-review and editing; all authors had approved the final version

REFERENCE

[1] B. He, S. Wang, and Y. Liu, "Underactuated robotics: A review," *Int. J. Adv. Robot. Syst.*, vol. 16, no. 4, 2019.

[2] G. Li, X. Liang, Y. Gao, T. Su, Z. Liu, and Z.-G. Hou, "A linkage-driven underactuated robotic hand for adaptive grasping and in-hand manipulation," *IEEE Trans. Autom. Sci. Eng.*, 2023.

[3] S. Parveen, M. Suhaib, and M. A. Majid, "Multifinger robotic gripper: A review," in *Proc. 2023 International Conference on Recent Advances in Electrical, Electronics & Digital Healthcare Technologies*, 2023, pp. 466–470.

[4] W. Chen and C. Xiong, "On adaptive grasp with underactuated anthropomorphic hands," *Journal of Bionic Engineering*, vol. 13, no. 1, pp. 59–72, 2016.

[5] R. J. Chauhan and P. Ben-Tzvi, "A series elastic actuator design and control in a linkage based hand exoskeleton," in *Proc. Dynamic Systems and Control Conference*, 2019, vol. 59162, V003T17A003.

[6] H. Yang, G. Wei, and L. Ren, "Design and development of a linkage-tendon hybrid driven anthropomorphic robotic hand," in *Proc. International Conference on Intelligent Robotics and Applications*, 2019, pp. 117–128.

[7] M. Askari, Y. Abbaspour-Gilandeh, E. Taghinezhad, A. M. El Shal, R. Hegazy, and M. Okasha, "Applying the Response Surface Methodology (RSM) approach to predict the tractive performance of an agricultural tractor during semi-deep tillage," *Agriculture*, vol. 11, no. 11, 1043, 2021.

[8] M. Askari, Y. Abbaspour-Gilandeh, E. Taghinezhad, R. Hegazy, and M. Okasha, "Prediction and optimizing the multiple responses of the Overall Energy Efficiency (OEE) of a tractor-implement system using response surface methodology," *J. Terramechanics*, vol. 103, pp. 11–17, 2022.

[9] H. C. Kwon, D. H. Cho, and K. H. Kim, "Underactuated three-finger robot hand with human-like flexion," *Int. J. Precis. Eng. Manuf.,* vol. 22, no. 5, pp. 791–798, 2021.

[10] X. V. Ha, C. Ha, and D. K. Nguyen, "A general contact force analysis of an under-actuated finger in robot hand grasping," *Int. J. Adv. Robot. Syst.*, vol. 13, no. 1, 2016.

[11] X. Chen, B. Peng, R. Huang, S. Wang, and Z. Yang, "Force distribution of thumb-index finger power-grasp during stable fruit grasp control," *Comput. Electron. Agric.*, vol. 198, 107058, 2022.

[12] D. Estay, A. Basoalto, J. Ardila, M. Cerda, and R. Barraza, "Development and implementation of an anthropomorphic underactuated prosthesis with adaptive grip," *Machines*, vol. 9, no. 10, 209, 2021.

[13] X. Li, Q. Huang, X. Chen, Z. Yu, J. Zhu, and J. Han, "A novel under-actuated bionic hand and its grasping stability analysis," *Adv. Mech. Eng.*, vol. 9, no. 2, 2017.

[14] S. R. Kashef, S. Amini, and A. Akbarzadeh, "Robotic hand: A review on linkage-driven finger mechanisms of prosthetic hands and evaluation of the performance criteria," *Mech. Mach. Theory*, vol. 145, 103677, 2020.

[15] Y. Bao and T. Takaki, "Manipulator equipped with differential wrist mechanism to combine the torque of two motors to increase fingertip force and wrist torque," *IEEE Robot. Autom. Lett.*, vol. 7, no. 4, pp. 10025–10032, 2022.

[16] Q. Liu, X. Gu, N. Tan, and H. Ren, "Soft robotic gripper driven by flexible shafts for simultaneous grasping and in-hand cap manipulation," *IEEE Trans. Autom. Sci. Eng.*, vol. 18, no. 3, pp. 1134–1143, 2020.

[17] M. M. Keller, R. Barnes, and C. Brandt, "Evaluation of grip strength and finger forces while performing activities of daily living," *Occup. Heal. South. Africa*, vol. 28, no. 5, pp. 187–191, 2022.

[18] F. J. Ruiz-Ruiz, J. Ventura, C. Urdiales, and J. M. Gómez-de-Gabriel, "Compliant gripper with force estimation for physical human–robot interaction," *Mech. Mach. Theory*, vol. 178, 105062, 2022.

[19] A. Carabello, R. Henkner, and W.-G. Drossel, "Novel procedure for determining the finger force in flexion depending on the finger position," *Current Directions in Biomedical Engineering*, vol. 8, no. 2, pp. 384–387, 2022.

[20] U. Kim, D. Jung, and H. Jeong *et al.*, "Integrated linkage-driven dexterous anthropomorphic robotic hand," *Nat. Commun.*, vol. 12, no. 1, pp. 1–13, 2021.

[21] E. H. Flaieh, H. G. Kamil, S. H. Bakhy, and M. A. Jabbar, "Design and analysis of multi-finger robotic hand," *J. Eng. Sci. Technol.*, vol. 16, no. 2, pp. 988–1005, 2021.

[22] D. Pei, P. Olikkal, T. Adali, and R. Vinjamuri, "Dynamical synergies of multidigit hand prehension," *Sensors*, vol. 22, no. 11, 4177, 2022.

[23] B. He, S. Wang, and Y. Liu, "Underactuated robotics: A review," *International Journal of Advanced Robotic Systems*, vol. 16, no. 4, 2019.

[24] M. B. Hong, S. J. Kim, Y. S. Ihn, G.-C. Jeong, and K. Kim, "KULEX-hand: An underactuated wearable hand for grasping power assistance," *IEEE Trans. Robot.*, vol. 35, no. 2, pp. 420–432, 2018.

[25] M. Chen, S. Li, F. Shuang, Y. Du, and X. Liu, "Development of a three-fingered multi-modality dexterous hand with integrated embedded high-dimensional sensors," *J. Intell. Robot. Syst.*, vol. 108, no. 2, 2023.

[26] G. Li, L. Cheng, Z. Gao, X. Xia, and J. Jiang, "Development of an untethered adaptive thumb exoskeleton for delicate rehabilitation assistance," *IEEE Trans. Robot.*, vol. 38, no. 6, pp. 3514–3529, 2022.

[27] K. DuFrene, "Comparing actuation and underactuation of robotic hands," Bachelor's thesis, Oregon State University, USA, 2022.

[28] G. Li, P. Xu, S. Qiao, and B. Li, "Stability analysis and optimal enveloping grasp planning of a deployable robotic hand," *Mech. Mach. Theory*, vol. 158, 104241, 2021.